Estimation of the Tire Cornering Stiffness as a Road Surface Classification Indicator Using Understeering Characteristics

Kyoungseok Han, Mooryong Choi, and Seibum B. Choi, *Member, IEEE*

***Abstract*—Real-time classification of road surface conditions is very important for the control of a vehicle properly within its handling limits. There have been numerous attempts to estimate the road surface conditions, but there is a plenty of room for improvement, since most of the estimation methods have some robustness issues in real-world applications. The method proposed in this paper utilizes the relationship between the road surface condition and the tire cornering stiffness. Since the tire cornering stiffness varies significantly depending on the road surface condition, it can be estimated out of the tire cornering stiffness, which is measured accurately at the early state of wheel slip. In this study, normalized tire cornering stiffnesses are estimated in real time, exploiting the fact that production vehicles are generally built to show some understeering characteristics. The proposed method compares the front and rear wheel slips simultaneously, unlike other studies that focus on individual wheel slip. In this way, estimation of unmeasurable major vehicle states such as wheel sideslip angle and absolute vehicle speed can be eliminated from the entire algorithm. The experimental results show satisfactory estimates of less than 10% error and confirm the feasibility of the proposed algorithm in production vehicles without exotic extra sensors.**

***Index Terms*—Tire-road friction coefficient, cornering stiffness, understeering characteristics, linear tire model and sideslip angle.**

I. Introduction

OVER the past few decades, a significant number of vehicle chassis control systems have been developed to provide sufficient assistance to drivers [1]–[3]. Among them, electronic stability control (ESC) systems have been designed to prevent the deviation of the current vehicle state from the desired value, and this is especially true for the yaw rate [1]. Given this benefit, the mandatory installation of ESC systems has become more common in the automotive manufacturing industry. Often, in order to manage numerous types of driving situations, the use of rule-based algorithms [4], [5] is becoming more widely accepted, but a significant computational burden is imposed. For this reason, several leading studies have focused on state feedback control methods with estimations of major vehicle states, such as the tire-road friction coefficient (TRFC) and/or the sideslip angle. With the assistance of these estimations, control actions can be taken if a specified amount of deviation from the current state is detected. However, this type of control strategy has an important limitation in that estimations of major vehicle states are typically difficult due to the limited number of sensors in production vehicles. Although numerous attempts have been made to estimate these states more accurately, the performance outcomes remain controversial.

Several researchers have stated that well-known mathematical nonlinear tire models encompass major vehicle states, such as the TRFC, sideslip angle, tire slip, and cornering stiffness. Therefore, the TRFC can also be identified given that the other parameters in the model are well expressed using affordable sensors in production vehicles. However, as mentioned above, the number of sensors in production vehicles are insufficient to accurately measure or estimate all the parameters of conventional tire models. In one area of research [6]–[10], inertial sensors or minimal additional sensors were utilized while considering the vehicle lateral dynamics in order to estimate the TRFC. Several other studies have estimated the sideslip angle [11]–[13], which can facilitate the expression of the lateral dynamic or mathematical tire model. It was also found to be useful to use the aligning moment as an excitation signal to estimate the TRFC [14], [15].

A common problem with the aforementioned studies is that the methods they present should satisfy the persistent excitation (PE) condition [16]. That is, sufficiently rich excitation signals, such as those associated with severe acceleration, deceleration, and the wheel steering angle, should be provided consistently. The classified TRFC can help a safety control system to predict reachable friction values in advance when the classification process is completed within the linear region of the tire force curve. Therefore, it is most desirable to classify the TRFC with a small excitation signal. However, this is very difficult in practice, which explains why the estimators developed thus far cannot be implemented in production vehicles. Moreover, inaccuracies in the estimated results, such as the sideslip angle at the intermediate level, can compound this problem.

This paper was motivated by longitudinal slip slope-based estimation methods [17]–[20], which have been shown to be

Manuscript received October 23, 2017; revised January 7, 2018 and February 13, 2018; accepted March 4, 2018. Date of publication March 27, 2018; date of current version August 13, 2018. This work was supported in part by the National Research Foundation of Korea (NRF) funded by the Korean Government (Ministry of Science, ICT, and Future Planning—MSIP) under Grant 2017R1A2B4004116; in part by the MSIP, South Korea, under the Information Technology Research Center support program supervised by the Institute for Information and Communications Technology Promotion under Grant IITP-2017-2012-0-00628; and in part by the BK21+ program through the NRF funded by the Ministry of Education of Korea. The review of this paper was coordinated by Dr. M.-S. Ahmed. *(Corresponding author: Seibum B. Choi.)*

K. Han and S. B. Choi are with the Korea Advanced Institute of Science and Technology, Daejeon 34141, South Korea (e-mail: hks8804@kaist.ac.kr; sbchoi@kaist.ac.kr).

M. Choi is with the Korea Railroad Research Institute, Uiwang 437-050, South Korea (e-mail: mucho@krri.re.kr).

Color versions of one or more of the figures in this paper are available online at http://ieeexplore.ieee.org.

Digital Object Identifier 10.1109/TVT.2018.2820094

0018-9545 © 2018 IEEE. Personal use is permitted, but republication/redistribution requires IEEE permission.
See http://www.ieee.org/publications_standards/publications/rights/index.html for more information.

Authorized licensed use limited to: Korea Advanced Inst of Science & Tech - KAIST. Downloaded on March 06,2020 at 10:35:29 UTC from IEEE Xplore. Restrictions apply.

useable in production vehicles. In earlier work [17]–[19], it was assumed that the TRFC could be represented by the longitudinal tire stiffness, with emphasis placed on estimating the tire stiffness in real time. However, the required accuracy level of the tire slip information needed to use this method cannot be obtained using currently equipped sensors in production vehicles. In other work [20], however, TRFC estimation was realized without measuring or estimating the tire slip. This was done by using the braking characteristics of production vehicles.

Similar to earlier work [17]–[19], this paper is based on the assumption that the TRFC can be ascertained by accurate estimations of the tire cornering stiffness. Therefore, it is assumed that the tire cornering stiffness can be distinguished according to the road surface condition, as in the longitudinal slip slope-based method [17]–[19]. As the basis for this claim, several attempts have been made to employ the cornering stiffness to classify the road surface condition [21]–[24]. However, the unmeasurable sideslip angle continues to complicate this task, and most studies separately deal with the estimating sideslip angle and the cornering stiffness. However, these two states are closely related, and inaccurate sideslip angle information gives an inaccurate cornering stiffness estimation result.

In order to resolve these technical shortcomings, a novel method is developed in this paper, motivated by earlier work [20] in which the necessity of the longitudinal tire slip information was eliminated when estimating the longitudinal tire stiffness by considering the braking characteristics of production vehicles. Similar to the braking characteristics, all passenger vehicles must be designed to have understeering characteristics for safety reason. This means that the wheel sideslip angles at the front wheels should always have a larger value than those for the rear wheels [25]. These handling characteristics are utilized to estimate the tire cornering stiffness, which is a core contribution of this paper.

Also, this paper is based on the concrete fact that tire force is proportional to the wheel sideslip angle within the linear region of the tire force curve. Hence, a linear tire model is utilized. From a practical standpoint, this is reasonable because safety systems can be satisfactorily assisted by the TRFC, which is classified within the linear region.

The rest of this paper is organized as follows. Section II presents the models utilized in this paper and estimation strategy. The performance of the developed algorithm is experimentally verified in Section III, and the paper is concluded in Section IV.

II. Tire Cornering Stiffness Estimation

A. Previous Approach

Fig. 1 presents an overview of a typical vehicle state estimation approach which has been widely introduced in the literature. The structure of the estimator can vary depending on the strategies, but the overall flow diagram does not deviate much from the figure above. The measured sensor signals are used to estimate the unmeasurable vehicle states like wheel sideslip angle and wheel longitudinal slip, and these estimates are substituted into the mathematical vehicle and tire model to get the tire parameters. In general, the estimation parts and the modeling parts are highly correlated, meaning that model-based estimators have been widely introduced in the literature. In these estimation processes, additional sensor signals are commonly used to measure the states required for their algorithms. However, using extra sensors need to be avoided in consideration of better cost competitiveness.

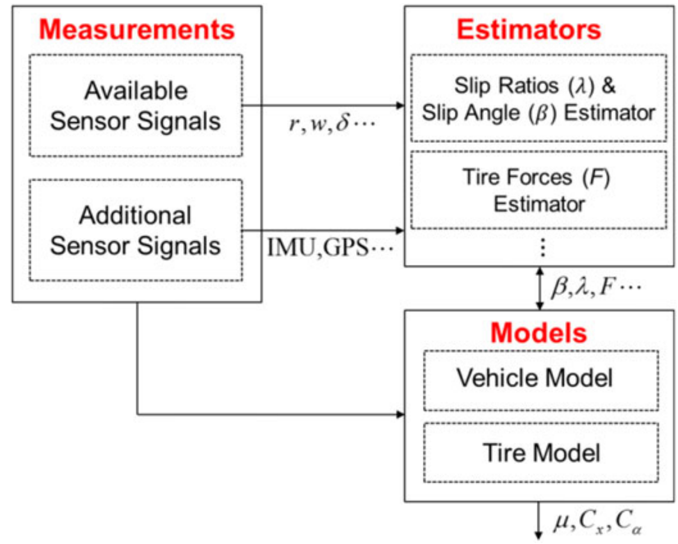

Fig. 1. Typical major vehicle state estimation approach.

Furthermore, the estimation performances of the tire parameters are significantly affected by inaccurate estimates of the tire slip ratio and slip angle at the intermediate step. If a chassis safety control system is designed based on these incorrect slip ratio and slip angle information, a serious safety issues can be occurred.

In this study, a simplified linear tire model is used since there is no major difference between a linear tire model and a nonlinear one within the linear region of the tire force curve. It should be noted that nonlinear tire models such as the magic formula, brush, and Dugoff tire models [26] are also formulated based on the fact that the tire force is linear with a range of small tire slip.

As noted earlier, it is desirable to classify the TRFC early in the linear region. Therefore, this linear region is an area of interest when estimating the TRFC. For this reason, a simplified linear tire model is sufficient enough to replace the nonlinear tire model. Accordingly, this paper employs a linear tire model. The behavior of the vehicle beyond the linear region is beyond the scope of the paper, but many of the previously developed methods have considered in this region [6]–[9].

In order to resolve the aforementioned problems, this paper presents a practice-oriented method motivated by earlier work [17]–[20]. That is, this paper shares a major strategy with the earlier studies, but it introduces a new way to eliminate the need for individual wheel sideslip angle estimations.

B. Proposed Approach

Fig. 2 describes the overall architecture of the proposed method. The primary difference that distinguishes Fig. 2 from Fig. 1 is that the individual sideslip angle estimator is removed in Fig. 2, and no extra sensor signals are used in Fig. 2. Note that complicated processes such as individual wheel sideslip angle estimations and identification of the vehicle weight are not part of the proposed method. This is possible by exploiting the understeering handling characteristics of production vehicles. In addition, compensated lateral tire forces in consideration of

Authorized licensed use limited to: Korea Advanced Inst of Science & Tech - KAIST. Downloaded on March 06,2020 at 10:35:29 UTC from IEEE Xplore. Restrictions apply.

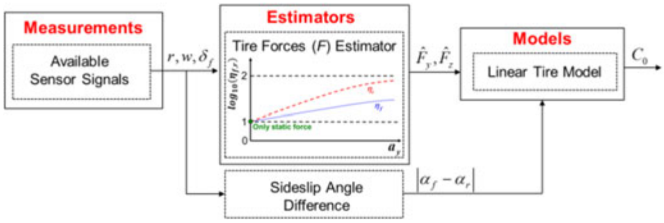

Fig. 2. Overall architecture of the proposed method.

weight transfer are introduced in Section II-D. From a practical perspective, implementing the proposed method in production vehicles is more feasible compared to previous methods due to the low computational effort and the low degree of dependence on extra sensors or additional intermediate-level estimation processes. The details are described in the following sections.

C. Vehicle Model

Since the method developed in this paper is based on the average vehicle major states of the right and left wheels, a bicycle model neglecting side-to-side weight shift is employed. The equations of motion in this model can be written as follows assuming a constant or slowly varying vehicle velocity [25],

$$\dot{\beta} = \frac{F_{\mathrm{yf}} + F_{\mathrm{yr}}}{m v_x} - r \tag{1}$$

$$\dot{r} = \frac{l_f F_{\mathrm{yf}} - l_r F_{\mathrm{yr}}}{I_z} \tag{2}$$

where β is the body sideslip angle, *m* is the vehicle gross weight, v_x is the vehicle velocity, *r* is the yaw rate, I_z is the yaw moment of inertia, F_{yf} and F_{yr} are correspondingly the front and rear axle lateral forces, and l_f and l_r are likewise the distances from the center of gravity to the front and rear axles.

The linear dynamic tire forces are determined as follows,

$$F_{\mathrm{yf,dynamic}} = -C_f \alpha_f \tag{3}$$

$$F_{\mathrm{yr,dynamic}} = -C_r \alpha_r \tag{4}$$

where C_f and C_r are the front and rear cornering stiffnesses, respectively, and α_f and α_r are the front and rear wheel sideslip angles, respectively.

It should be noted that (3) and (4) are valid when the vehicle is in the linear region of the tire force curve, which is the area of interest of this study.

Substituting (3) and (4) into the bicycle model, the system can be written in state-space form as $\dot{x} = Ax + B\delta_f$, where $x = [\beta \; r]^T$ and where the following holds:

$$A = \begin{bmatrix} -\frac{C_f + C_r}{m v_x} & \frac{C_r l_r - C_f l_f}{m v_x} - 1 \\ -\frac{C_r l_r - C_f l_f}{I_z} & -\frac{C_f l_f^2 + C_r l_r^2}{I_z} \end{bmatrix}$$

$$B = \begin{bmatrix} \frac{C_f}{m v_x} \\ \frac{C_f l_f}{I_z} \end{bmatrix} \tag{5}$$

In the simplified linear tire model of (3) and (4), the cornering stiffness is a key parameter needed to determine the lateral tire force accurately. Therefore, numerous efforts have been made to estimate the cornering stiffness in real time. Variation of the tire cornering stiffness according to the road surface condition was confirmed in earlier work [21]–[24].

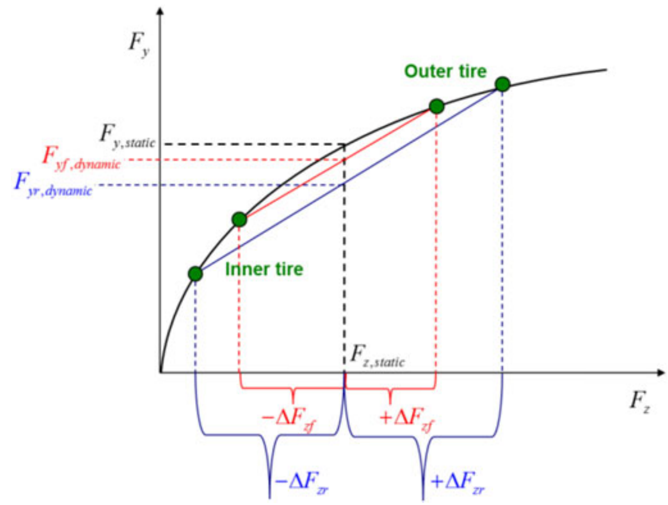

Fig. 3. Effects of a lateral load transfer on the resulting axle characteristics.

In general, the tire cornering stiffness for steady-state cornering can be expressed with consideration of static normal forces as follows [11], [26].

$$C_f = C_{f0}(\mu) \cdot F_{\mathrm{zf,static}} \tag{6}$$

$$C_r = C_{r0}(\mu) \cdot F_{\mathrm{zr,static}} \tag{7}$$

where $C_{f0}(\mu)$ and $C_{r0}(\mu)$ are the front and rear normalized cornering stiffnesses, which vary according to the road surface friction; $F_{\mathrm{zf,static}}$ and $F_{\mathrm{zr,static}}$ are the front and rear static normal forces; and μ is the road surface friction coefficient

Because the bicycle model, unable to consider the left and right wheels separately, is used, the tire cornering stiffnesses are normalized relative to the static normal forces. In (6) and (7), the normalized cornering stiffness varies based on the normal force and the TRFC within the linear region, and the front and rear wheels have nearly identical values if the vehicle is on a homogeneous road surface; i.e., $C_0(\mu) = C_{f0}(\mu) \approx C_{r0}(\mu)$, forming the basis of this study. However, this is not always valid because there are numerous other factors that affect the magnitude of the tire cornering stiffness. Therefore, (6) and (7) should be modified considering the lateral load transfer effect.

D. Lateral Load Transfer Effect

In (6) and (7), the static normal forces simply determined by the weight distribution of the vehicle were used. In reality, however, there are always lateral load transfers due to lateral acceleration at the center of gravity. The magnitude of a load transfer due to lateral acceleration is written as follows [27],

$$\Delta F_z = m a_y \frac{h}{t} \tag{8}$$

where a_y is the lateral acceleration, *h* is the height of the center of gravity, and *t* is the track width.

Considering the load transfer effect, the outer tire normal force is calculated by adding (8) to the static normal force, whereas the inner tire normal force is decreased by the amount of (8). In general, the lateral tire force is significantly influenced by these normal force variations [26]. As depicted in Fig. 3, the magnitudes of the dynamic lateral tire forces, i.e., $F_{\mathrm{yf,dynamic}}$, $F_{\mathrm{yr,dynamic}}$, are smaller than the static values without a lateral

Authorized licensed use limited to: Korea Advanced Inst of Science & Tech - KAIST. Downloaded on March 06,2020 at 10:35:29 UTC from IEEE Xplore. Restrictions apply.

load transfer. That is, the affordable lateral tire force is reduced due to the load transfer effect. Because the bicycle model, which does not consider side-to-side weight shifting, is used in this paper, the virtual static lateral tire forces, i.e., $F_{\text{yf,static}}$, $F_{\text{yr,static}}$, corresponding to the static normal force is introduced.

Fig. 3 indicates that the transferred load amounts for the front and rear tires differ, but (8) cannot provide a clear explanation of this phenomenon, as the roll bar stiffness effect is not considered in (8). In general, a stiffer roll bar allows a larger lateral load transfer, and Fig. 3 shows an example where the rear roll bar stiffness is larger than that at the front. In the automotive industry, the sum of front and rear roll stiffnesses is generally constant, and the ratio between the front and rear axles is distributed. Fortunately, the stiffnesses of the front and rear roll bar are tuned to have constant values which do not change unless the roll bar is replaced. Therefore, if the load transfer amount is determined by the lateral acceleration in (8), it can be assumed that the front-to-rear distribution ratio of the roll stiffness is always constant.

This paper assumes that the reduction in the lateral tire force is mainly due to the lateral acceleration and roll bar stiffness settings for the front and rear axles. However, constant values for the roll bar stiffnesses are specified. Therefore, the following correction factors can be introduced to determine the virtual static lateral forces,

$$F_{\text{yf,static}} = \eta_f\left(a_y\right)\cdot F_{\text{yf,dynamic}} \tag{9}$$

$$F_{\text{yr,static}} = \eta_r\left(a_y\right)\cdot F_{\text{yr,dynamic}} \tag{10}$$

where η_f and η_r are the front and rear correction factors which are the function of a_y.

The introduced correction factors can be experimentally determined and expressed in the form of a look-up table. This will be described in Section II-E.

E. Linear Tire Model

The wheel sideslip angle for the front and rear wheels can be written as follows [25],

$$\alpha_f = \beta + \frac{l_f}{v_x} r - \delta_f \tag{11}$$

$$\alpha_r = \beta - \frac{l_r}{v_x} r \tag{12}$$

where δ_f is the steered wheel angle.

Dividing (3) and (4) with normal forces leads to the following,

$$\frac{F_{\text{yf,static}}}{F_{\text{zf,static}}} = -\frac{\eta_f\left(a_y\right)C_f}{F_{\text{zf,static}}}\alpha_f = -\eta_f\left(a_y\right)C_0\left(\mu\right)\alpha_f \tag{13}$$

$$\frac{F_{\text{yr,static}}}{F_{\text{zr,static}}} = -\frac{\eta_r\left(a_y\right)C_r}{F_{\text{zr,static}}}\alpha_r = -\eta_r\left(a_y\right)C_0\left(\mu\right)\alpha_r \tag{14}$$

These linear tire models for the front and rear wheels are utilized in last block of Fig. 2. As mentioned, if the front and rear wheels are assumed to follow the same road surface, the normalized cornering stiffness is identical in each wheel. Therefore, the estimated normalized cornering stiffness can be an indicator with which to classify the road surface condition, as shown in Fig. 4 [24], [28].

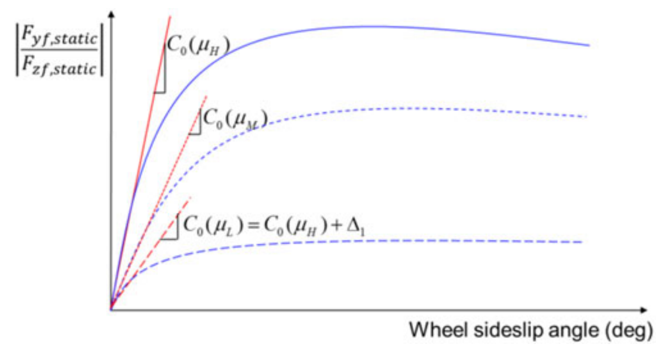

Fig. 4. Normalized lateral tire force curve: μ_H, μ_M, and μ_L are the high, medium, and low tire–road friction coefficients, respectively.

F. Estimation Strategy

In this sub-section, a central part of this study is introduced. It should be noted here that the proposed method makes three major assumptions.

First, the front and rear tires are identical to each other, implying that their normalized cornering stiffnesses are identical. Second, the vehicle is traveling on a homogenous road surface at a constant velocity. That is, all wheels experience the same road surface condition. Finally, the vehicle does not have neutral steering characteristics, which is true for production vehicles.

Note that the normalized cornering stiffness can easily be determined from (13) and (14), as follows:

$$C_0\left(\mu\right) = -\frac{1}{\eta_f\left(a_y\right)\alpha_f}\cdot\frac{F_{\text{yf,static}}}{F_{\text{zf,static}}} = -\frac{1}{\eta_r\left(a_y\right)\alpha_r}\cdot\frac{F_{\text{yr,static}}}{F_{\text{zr,static}}} \tag{15}$$

Combining (1) and (2), the lateral tire force of each axle is represented as shown below. These values can be calculated easily using the vehicle inertial parameters and sensor signals.

$$F_{\text{yf,dynamic}} = \frac{ml_r a_y + I_z\dot{r}}{l_f + l_r}$$
$$F_{\text{yr,dynamic}} = \frac{ml_f a_y - I_z\dot{r}}{l_f + l_r} \tag{16}$$

Furthermore, the static normal tire forces, which are constant, can be calculated using the equation shown below.

$$F_{\text{zf,static}} = mg\frac{l_r}{l_f + l_r}$$
$$F_{\text{zr,static}} = mg\frac{l_f}{l_f + l_r} \tag{17}$$

where g is the gravitational constant.

As compared to the sideslip angles, the normalized tire forces can be estimated with relative ease.

Using (16) and (17), the normalized tire force can be expressed as follows:

$$\frac{F_{\text{yf,static}}}{F_{\text{zf,static}}} = \eta_f\left(a_y\right)\frac{ml_r a_y + I_z\dot{r}}{mgl_r}$$
$$\frac{F_{\text{yr,static}}}{F_{\text{zr,static}}} = \eta_r\left(a_y\right)\frac{ml_f a_y - I_z\dot{r}}{mgl_f} \tag{18}$$

Given that the yaw moment of the inertia is a function of the vehicle mass, as in (19), the normalized forces estimated in (18)

Authorized licensed use limited to: Korea Advanced Inst of Science & Tech - KAIST. Downloaded on March 06,2020 at 10:35:29 UTC from IEEE Xplore. Restrictions apply.

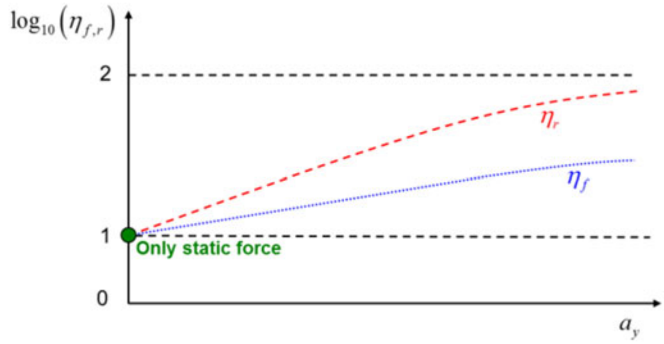

Fig. 5. Correction factor curve according to the lateral acceleration.

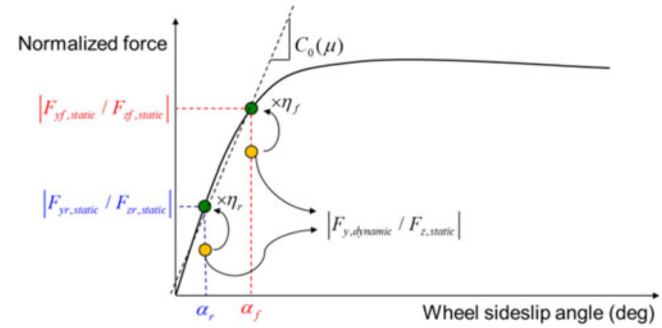

Fig. 6. Normalized lateral tire force curve: $F_{\mathrm{yf}}/F_{\mathrm{zf}}$ and $F_{\mathrm{yr}}/F_{\mathrm{zr}}$ are the front and rear normalized forces.

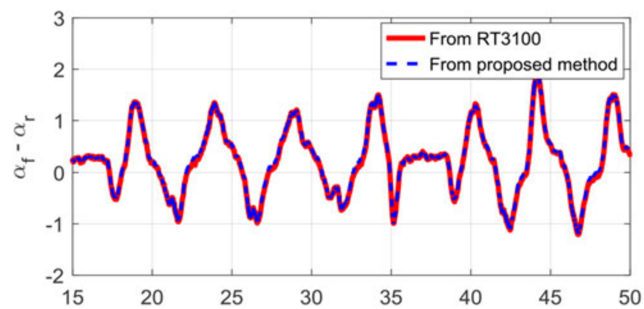

Fig. 7. Comparison of the wheel sideslip difference with sine steering on dry asphalt.

can be said to be free from the vehicle gross mass error,

$$I_z = m\bar{k}^2 \tag{19}$$

Here, $\bar{k}^2$ is the radius of gyration, which is assumed to be known.

The correction factors, i.e., η_f and η_r, are determined from the lookup table in Fig. 5. The measured value of a_y can be used to obtain the correction factors corresponding to the front and rear wheels. Fig. 5 can be predefined through experiments involving a wide range of vehicle lateral acceleration levels. Using the RT3100 device, which can measure the sideslip angle accurately, Fig. 4 is established by compensation with (15).

That is, the open-loop calculations of (16) are compared with the $-C_f\alpha_f$ and $-C_r\alpha_r$ which are regarded as actual lateral tire forces, and the dynamic forces of (16) are compensated by the correction factors. In this process, the nominal values of C_f and C_r in a specific road condition are utilized to calculate the true lateral tire forces. As noted above, the roll stiffness of the front and the rear axles is a fixed value; hence, a single well-made experiment is sufficient to create the lookup table before releasing the vehicle.

Although the calculated normalized tire forces describe the actual values well, estimating the individual wheel sideslip angles in (15) remains a challenge. Previously, numerous attempts to obtain accurate sideslip values were reported, but there is little agreement on the estimation performance outcomes. In this paper, a novel method that is free from the effect of sideslip error is proposed using the understeering characteristics of production vehicles.

It is well recognized that most vehicles should be designed to have understeering characteristics during steady-state cornering [25]. That is, the value of the wheel sideslip angle at the front wheel should be larger than those for the rear wheels, as depicted in Fig. 6. If the wheel sideslip angles at the rear wheels reach the saturation point first, the vehicle goes into oversteering area; this is the most critical condition to be prevented. However, understeering is the opposite of oversteering and is allowed to a certain extent during actual driving. For this reason, production vehicles are usually tuned to have understeering-biased handling characteristics by adjusting the nominal front and rear cornering stiffness and mass distribution values [25].

Once a driver begins to steer the vehicle, it is guaranteed that there is a sideslip difference between the front and rear wheels due to the abovementioned characteristics. Moreover, it is well known that the normalized lateral tire force curve maintains a linear trajectory with a small slip angle.

In addition, the difference in the sideslip angle between the front and rear wheels can be calculated using (11) and (12):

$$\alpha_f - \alpha_r = \frac{l_f + l_r}{v_x} r - \delta_f \tag{20}$$

This slip angle difference is exploited to replace the individual sideslip angle estimation in Fig. 1, as illustrated in overall algorithm structure of Fig. 2.

As shown in Fig. 6, (15) can be expressed within a linear region as follows,

$$\begin{aligned} C_0(\mu) &= \left| \frac{F_{\mathrm{yf,static}}/F_{\mathrm{zf,static}} - F_{\mathrm{yr,static}}/F_{\mathrm{zr,static}}}{\alpha_f - \alpha_r} \right| \\ &= \frac{\left|F_{\mathrm{yf,static}}/F_{\mathrm{zf,static}} - F_{\mathrm{yr,static}}/F_{\mathrm{zr,static}}\right|}{\left|\frac{l_f + l_r}{v_x} r - \delta_f\right|} \end{aligned} \tag{21}$$

It can be observed in (21) that the proposed method is effective if there is a slip angle difference between the front and rear wheels. That is, (21) is always supported if the vehicle does not exhibit neutral steering characteristics [25]. However, the main purpose of TRFC classification is to provide an estimate within the linear region where the vehicle exhibits understeering characteristics. Therefore, the basic principle of this paper is based on understeering characteristics.

It is important to note that the necessity of the sideslip estimation is eliminated and that readily available signals in production vehicles are sufficient to express the normalized cornering stiffness in (21).

In order to verify these characteristics, experiments were conducted using a production vehicle. Fig. 7 describes the comparison of the measured $\alpha_f - \alpha_r$ values with those calculated

Authorized licensed use limited to: Korea Advanced Inst of Science & Tech - KAIST. Downloaded on March 06,2020 at 10:35:29 UTC from IEEE Xplore. Restrictions apply.

using the proposed method in (20) for sine steering input on dry asphalt. The measured value was from RT3100, a high-accuracy vehicle dynamic testing device; the results were obtained from the measured signal as follows,

$$\alpha_f = \tan^{-1}\left(\frac{v_y}{v_x} + \frac{l_f}{v_x} r\right) - \delta_f,\ \alpha_r = \tan^{-1}\left(\frac{v_y}{v_x} - \frac{l_r}{v_x} r\right) \tag{22}$$

where v_x and v_y are longitudinal and lateral velocity, respectively, as obtained from RT3100 with high accuracy. As shown in Fig. 7, it can be concluded that the value from the proposed method is in very good agreement with the actual value.

In order to reduce the noise effect, the recursive least square (RLS) algorithm is applied for the system $y(t)\theta(t) \cdot \phi(t)$. The calculations at each step *t* are as follows [29],

Step 1: Measure or calculate the system output y(t) and regression $\phi(t)$.

Step 2: Calculate the updated gain, $K(t)$ and covariance $P(t)$, as

$$K(t) = \frac{P(t-1)\,\phi(t)}{\lambda + P(t-1)\,\phi^2(t)} \tag{23}$$

$$P(t) = \frac{1}{\lambda}\left[P(t-1) - \frac{P^2(t-1)\,\phi^2(t)}{\lambda + P(t-1)\,\phi^2(t)}\right] \tag{24}$$

Step 3: Update the parameter estimate, as follows,

$$\hat{\theta}(t) = \hat{\theta}(t-1) + K(t)\left\{y(t) - \hat{\theta}(t-1)\,\phi(t)\right\} \tag{25}$$

where

$$y = \left|\frac{F_{\mathrm{yf,static}}}{F_{\mathrm{zf,static}}} - \frac{F_{\mathrm{yr,static}}}{F_{\mathrm{zr,static}}}\right|, \theta = C_0(\mu) \text{ and}$$

$$\phi = \left|\frac{l_f - l_r}{v_x} r - \delta_f\right|.$$

The forgetting factor (λ) that is used to reduce the influence of previous data is a function of the time derivative of the steering wheel angle: $\lambda(\dot{\delta}_f)$. In general, when the forgetting factor is smaller, a faster convergence rate is guaranteed. However, severe oscillation can be caused by a small λ. This tradeoff is used in this paper.

As stated above, the TRFC should be estimated sufficiently early because the ultimate goal of this study is to predict the maximum reachable tire force with a small excitation signal. When the vehicle is in a mild driving situation while the lateral tire force remains in the linear region of the lateral tire force curve, only a small value of the time derivative of steering wheel angle is detected. At this time, a more accurate estimation of the TRFC without fluctuation can be achieved by employing a large value of the forgetting factor because a faster convergence rate with a certain level of fluctuation of the estimated value is not preferred in this situation.

In other words, there is sufficient time to approach the peak point in the lateral tire force curve when the vehicle drives mildly; therefore, a more accurate estimate is desirable in this case.

However, the TRFC should be identified quickly with a small value of the forgetting factor when the steering angle sensor signal shows a large value of $\dot{\delta}_f$. Because the vehicle may reach the inherent limitation quickly in this maneuver, the forgetting factor must be adjusted to a small value to allow a rapid change of the estimated value.

(a) (b)

Fig. 8. (a) Test vehicle (compact SUV). (b) RT 3100 installed inside the vehicle.

TABLE I
TEST VEHICLE AND TIRE MODEL SPECIFICATIONS

Parameters	Quantity	Values
m	Gross vehicle weight (2UP)	1673 kg
l_f	Distance between the front axle and center of gravity	0.91 m
l_r	Distance between the rear axle and center of gravity	1.73 m
I_z	Yaw moment of inertia of a vehicle	3484 kg $\cdot$ m^2
h	Height of center of gravity	0.615 m
t	Track width	1.585 m
C_f	Front cornering stiffness at dry asphalt	90000 N/rad
C_r	Rear cornering stiffness at dry asphalt	55000 N/rad

III. Experimental Results

A. Experimental Setup and A Priori Estimate

In order to confirm the performance of the proposed method, experiments were conducted using a test vehicle on a proving ground. The data was obtained using a CANBUS monitoring system; the proposed algorithm was operated with a 200 Hz sampling frequency, and no computational burden was found.

Fig. 8(a) is a photograph of the test vehicle, and Fig. 8(b) describes the RT3100 installed inside the test vehicle. Also, Table I gives the specifications of the test vehicle and the tire models which are the same as those of a commercially available vehicle. The true vehicle states, e.g., the vehicle lateral and longitudinal speeds, were measured using the RT3100 device but were unknown to the proposed algorithm. The experiments were performed on two types of road surfaces: dry asphalt and packed snow. Before verification of the proposed method, static a *priori* values of the surface properties were obtained using (15). It may be argued that the basis of the proposed algorithm becomes invalid if the calculated normalized cornering stiffness at the front and rear wheels have different values on the same road surface. In order to avoid such criticism, open-loop calculations of C_{f0} and C_{r0} using the velocities measured by RT3100 were conducted. In addition, C_o calculated from (21) was obtained, as depicted in Fig. 9.

That is, this test was designed to ensure that C_0, C_{f0} and C_{r0} had nearly identical values given that the vehicle was traveling

Authorized licensed use limited to: Korea Advanced Inst of Science & Tech - KAIST. Downloaded on March 06,2020 at 10:35:29 UTC from IEEE Xplore. Restrictions apply.

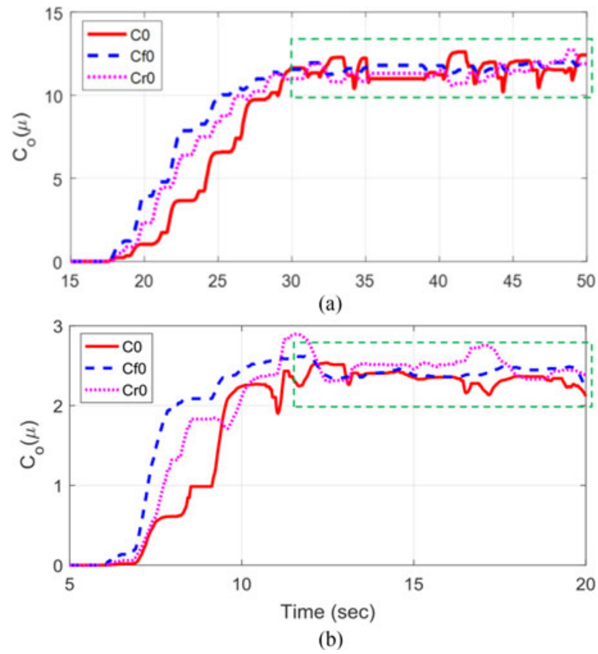

Fig. 9. Sine steering results. (a) Calculated C_0, C_{f0}, and C_{r0} on dry asphalt. (b) Calculated C_0, C_{f0}, and C_{r0} on packed snow.

on a homogenous surface. Moreover, the normalized cornering stiffnesses should be distinguished on different road surfaces.

The sinusoidal driver steering input was generated and the RLS algorithm was applied to (15) and (21) with a high forgetting factor, which can reduce the noise effect from the sensor signals because the objective of this test was to make the static *a priori* estimate of the surface properties and not to obtain real-time information about the road surface properties.

As illustrated in Fig. 9(a), the values of C_{f0} and C_{r0} on dry asphalt converged to about 12 for both wheels and it was also confirmed that the estimated value of the proposed method, i.e., C_0, was identical to the values of C_{f0} and C_{r0}.

Therefore, it can be concluded that the proposed method is promising because the obtained C_0 is similar to $C_{r0}(\mu_H)$ and $C_{f0}(\mu_H)$ on dry asphalt; this was proven, as described in Fig. 9(a).

Similar to this test, the vehicle was driven on packed snow with a sine steering maneuver in order to identify the properties of the packed snow road surface. As illustrated in Fig. 9(b), the identified values were about 2.5. Therefore, it can be concluded that the obtained normalized cornering stiffnesses on different road surfaces were sufficient to distinguish the TRFC, and the basic principle of this paper is supported by these tests.

As illustrated in Fig. 10, a quantitative relationship between C_o and TRFC can be predefined by these tests for different road surface conditions.

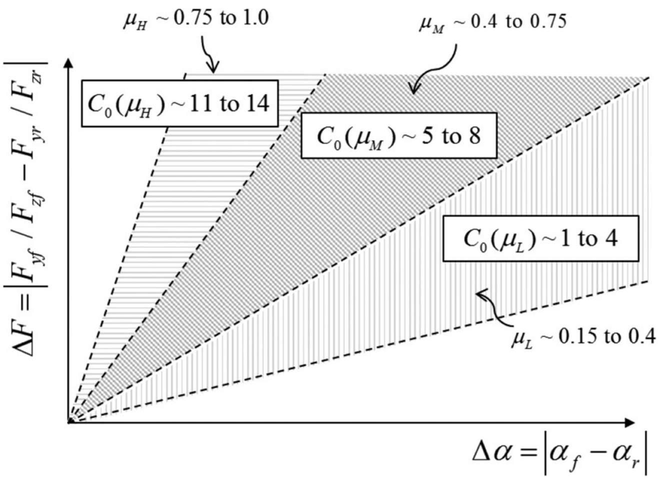

Fig. 10. Quantitative relationship between normalized cornering stiffness and TRFC.

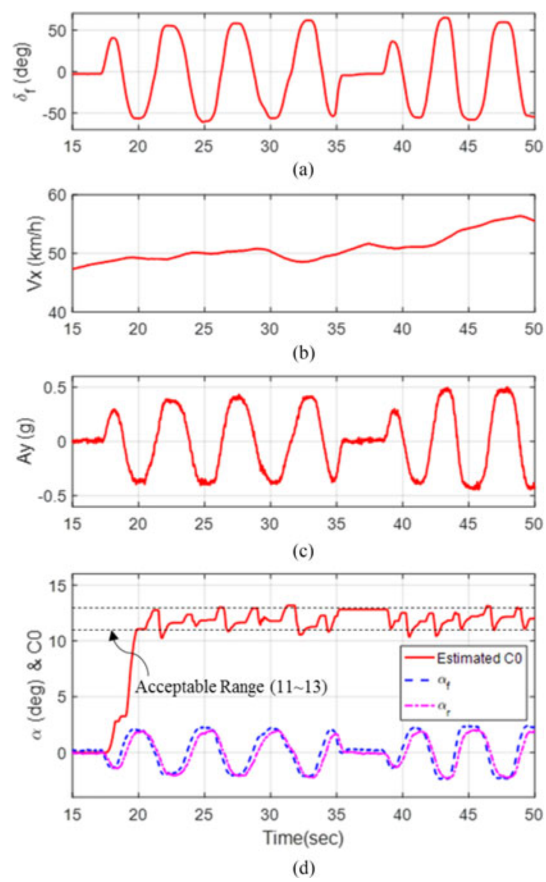

Fig. 11. Light sine steering results on dry asphalt. (a) Steering wheel angle, (b) velocity, (c) lateral acceleration, and (d) wheel sideslip angles and estimated normalized cornering stiffness.

B. Test Results

The first test scenario was conducted on dry asphalt with a light sine steering maneuver. Fig. 11(a) indicates that the driver command reached approximately 50°, and it describes a light turn during actual driving. The intent of this experiment was to capture the observer performance, even if a small excitation signal, e.g., δ_f, was given, which is the ultimate goal of the proposed method. The vehicle was accelerated to and maintained at a constant velocity of approximately 50 km/h, as described in Fig. 11(b). This constant velocity implies that the longitudinal tire force contributed little to form the friction force. Therefore, the longitudinal dynamic was ignored and only the lateral acceleration was considered, as depicted in Fig. 11(c). With the small excitation signal, the vehicle generated friction

Authorized licensed use limited to: Korea Advanced Inst of Science & Tech - KAIST. Downloaded on March 06,2020 at 10:35:29 UTC from IEEE Xplore. Restrictions apply.

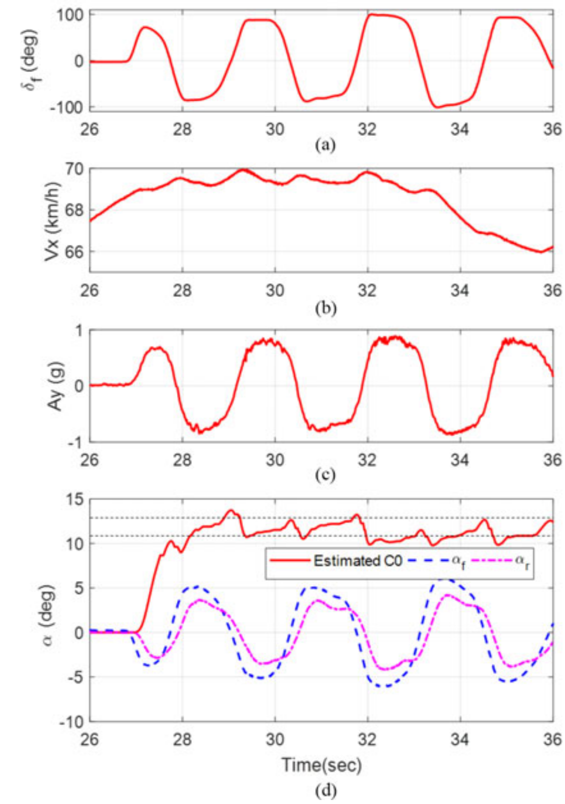

Fig. 12. Severe sine steering results on dry asphalt. (a) Steering wheel angle, (b) velocity, (c) lateral acceleration, and (d) wheel sideslip angles and estimated normalized cornering stiffness.

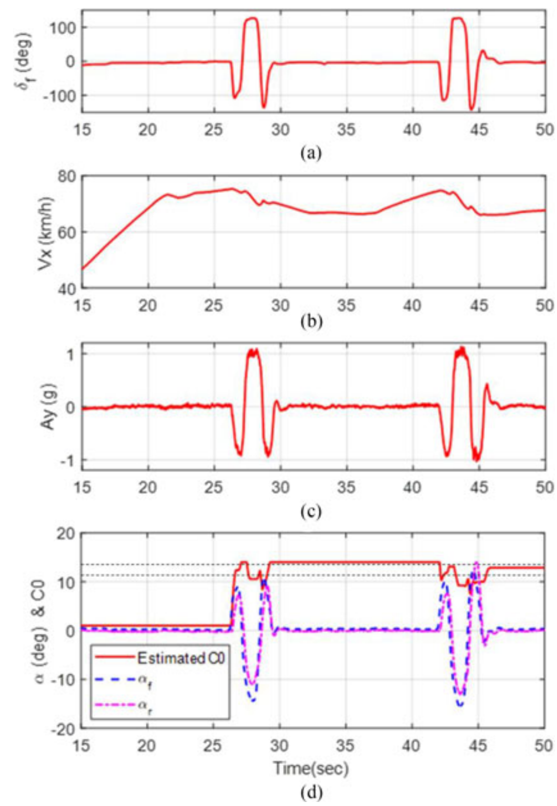

Fig. 13. Double lane change on dry asphalt. (a) Steering wheel angle, (b) velocity, (c) lateral acceleration, and (d) wheel sideslip angles and estimated normalized cornering stiffness.

force of less than $0.4g$, although the road surface could provide up to $1g$. This implies that information about the maximum reachable friction force was not provided to the vehicle as the acceleration was measured. However, the proposed method can provide useful information with the identified normalized cornering stiffness. As discussed above, the front wheel sideslip angles increased more rapidly than those for the rear wheels due to the understeering characteristics, as illustrated in Fig. 11(d).

Using these characteristics, the normalized cornering stiffness value was found to be approximately 12, identical to that in Fig. 9(a), and remained within the acceptable range (11–13) for a dry asphalt. Furthermore, the convergence rate was fast enough to estimate the TRFC in real time. As depicted in Fig. 11(d), driver steering input was exerted at approximately $t = 17$ sec, and the estimated C_0 had already converged to the true value. Unlike the results of Fig. 9(a), a small value of the forgetting factor was applied to obtain fast convergence result. Therefore, a certain amount of fluctuation was inevitable.

In order to filter the estimation results, some threshold settings were specified. For example, the algorithm begins to stop when the (20) exhibits a small sideslip angle difference because a very small excitation signal, i.e., $|\alpha_f - \alpha_r|$, can cause some divergence. Once the TRFC is determined by the appropriate amount of excitation signal, the normalized forces, i.e., μ_f, μ_r, are also monitored in real time to hold the results to the estimates of the previous step when the vehicle is about to enter the nonlinear region of the tire force curve. This is because only linear region is the area of interest.

Similarly to the first test scenario, the vehicle was maneuvered on flat dry asphalt. However, the steering command was increased significantly. The measured steering wheel angle in Fig. 12(a) describes a conventional slalom test, and the maximum value was approximately 100°. The vehicle velocity was also increased, as described in Fig. 12(b), and a certain level of variation in the velocity was observed. However, this situation did not require modification of the algorithm because the vehicle velocity varied slowly. Therefore, the proposed method remains effective unless brake force is exerted. It would be interesting to consider the combined effects of the longitudinal and lateral dynamics in this research, but this is beyond the scope of this study.

The increased steering wheel angle resulted in an increase in the lateral acceleration, as depicted in Fig. 12(c). It can be interpreted that the tire force nearly reached its saturation point. However, the vehicle did not become unstable due to an appropriate counter-steering maneuver. As expected, the identified values of the normalized cornering stiffness in Fig. 12(d), i.e., approximately 12, can describe the dry asphalt surface very well, and this corresponds to the static *a priori* estimation value in Fig. 9(a).

To verify the effectiveness of the specified thresholds, a more severe steering input was applied, as shown in Fig. 13(a). This is the input of the double lane change (DLC) test designed to confirm the lateral stability of vehicle. Since the steering wheel increased rapidly enough to reach the nonlinear region, the algorithm maintains the estimated value while the vehicle is in the nonlinear region or very small sideslip region. Due to

Authorized licensed use limited to: Korea Advanced Inst of Science & Tech - KAIST. Downloaded on March 06,2020 at 10:35:29 UTC from IEEE Xplore. Restrictions apply.

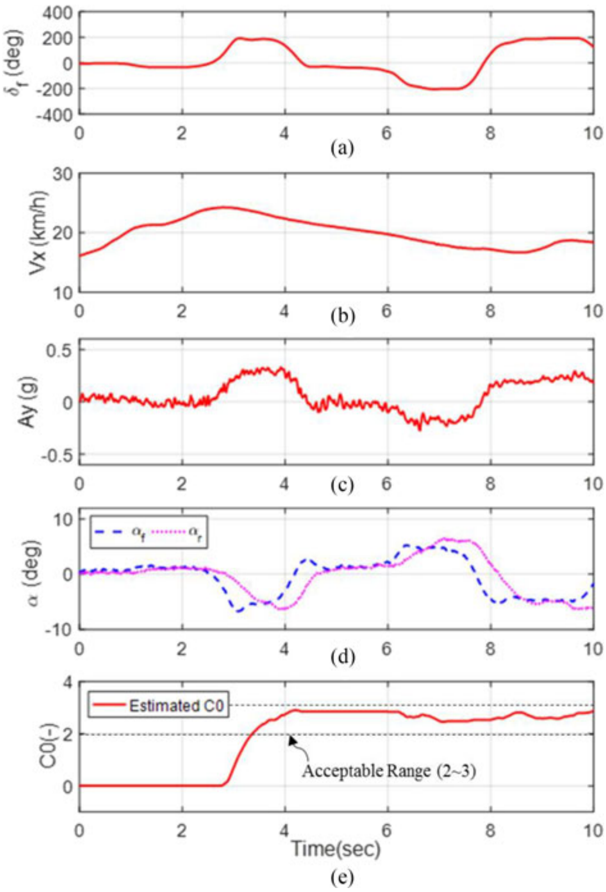

Fig. 14. Sine steering results on packed snow. (a) Steering wheel angle, (b) velocity, (c) lateral acceleration, (d) wheel sideslip angles, and (e) estimated normalized cornering stiffness.

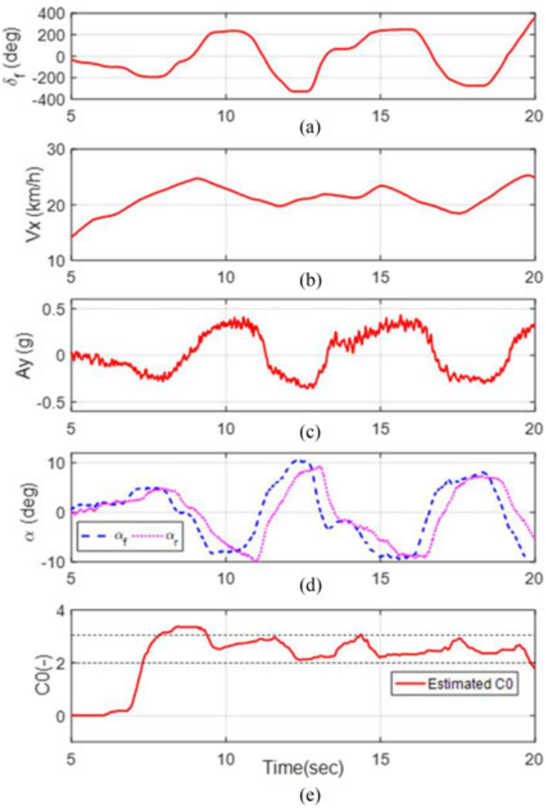

Fig. 15. Severe sine steering results on packed snow. (a) Steering wheel angle, (b) velocity, (c) lateral acceleration, (d) wheel sideslip angles, and (e) estimated normalized cornering stiffness.

this maneuver, the larger wheel sideslip angles greater than the those of the previous tests were observed in Fig. 13(d).

Fig. 13(d) shows that the estimation process was completed with an appropriate amount of excitation signal, and was often maintained at the previous value by discarding the signals that exceeded the specified thresholds. Therefore, it can be concluded that the specified thresholds performed the signal processing appropriately.

In the fourth test, the behavior of the vehicle on a packed snow road surface was investigated. As defined above, the normalized cornering stiffness on this road surface was significantly lower than those for asphalt. In order to verify these road properties, steering input was conducted, as illustrated in Fig. 14(a). In this test, several lane changes were included. The front wheel sideslip angle in Fig. 14(d) increased faster than that of the rear as in the dry asphalt. Fig. 14(b) presents the velocity, and the lateral acceleration was limited by the road surface properties, as depicted in Fig. 14(c).

Although a larger sideslip angles of Fig. 14(d) occurred compared to those of dry asphalt due to the severe maneuver, a smaller lateral acceleration was generated due to the reduced road friction coefficient. In general, it is well known that a surface such as that in this test provides a value of μ in a range of 0.3–0.4. As depicted in Fig. 14(c), the test vehicle nearly reached the physical boundary. Note that the proposed algorithm was suspended when the tires went into the nonlinear area in the lateral tire force curve because the basic principle of this paper becomes invalid if linearity is not guaranteed. Therefore, a threshold was set to judge the linearity, and the identified value was assumed to be the normalized cornering stiffness. The identified value, i.e., approximately 2.5, corresponds to that in Fig. 9(b).

Fig. 15 describes an experiment results with severe sine steering on packed snow, and it exhibited a pattern similar to that in Fig. 14. Because the test was performed on the same road surface using the same test vehicle, the estimated normalized cornering stiffness in Fig. 15(e) had a value that was nearly identical to that in Fig. 14(e). However, the algorithm was frequently suspended due to the severe excitation signal, which was reasonable when considering the goal of this paper.

In summary, although some fluctuations were observed in all test results, it was possible to distinguish dry asphalt and packed snow road surfaces using the proposed method. Therefore, it is anticipated that different types of TRFC can be determined in real-time by constructing the C_0 and μ to look-up table for a target vehicle. In this way, the identified C_0 can correspond to the value of the assigned μ in the constructed look-up table.

IV. Conclusion

This paper presented a novel strategy for classifying the TRFC without additional intermediate level estimations. The core principle of the proposed method is that most production vehicles are designed to have understeering characteristics for safety reasons. Using the developed algorithm, a more active chassis control system that utilizes the maximum road surface

Authorized licensed use limited to: Korea Advanced Inst of Science & Tech - KAIST. Downloaded on March 06,2020 at 10:35:29 UTC from IEEE Xplore. Restrictions apply.

properties is anticipated. In summary, it is concluded that the proposed method can be an indicator with which to classify the TRFC without estimating or measuring the sideslip angle. This is the major contribution of this paper. The test results reveal that the developed indicator is a promising tool, alongside more practice-oriented aspects. Regarding price competiveness, it was demonstrated that the proposed algorithm could be implemented in a production vehicle without extra costs. In addition, it is expected that the developed algorithm can be used for autonomous vehicle technologies because the road surface environments needs to be monitored in real-time in high level of driving automation.

References

[1] M. Choi and S. B. Choi, "Model predictive control for vehicle yaw stability with practical concerns," *IEEE Trans. Veh. Technol.*, vol. 63, no. 8, pp. 3539–3548, Oct. 2014.

[2] K. Han, M. Choi, B. Lee, and S. B. Choi, "Development of a traction control system using a special type of sliding mode controller for hybrid 4WD vehicles," *IEEE Trans. Veh. Technol.*, vol. 67, no. 1, pp. 264–274, Jan. 2018.

[3] A. Patil, D. Ginoya, P. Shendge, and S. Phadke, "Uncertainty-estimation-based approach to antilock braking systems," *IEEE Trans. Veh. Technol.*, vol. 65, no. 3, pp. 1171–1185, Mar. 2016.

[4] C. Geng, L. Mostefai, M. Denaï, and Y. Hori, "Direct yaw-moment control of an in-wheel-motored electric vehicle based on body slip angle fuzzy observer," *IEEE Trans. Ind. Electron.*, vol. 56, no. 5, pp. 1411–1419, May 2009.

[5] K. J. Åström, *Introduction to Stochastic Control Theory*. North Chelmsford, MA, USA: Courier Corp., 2012.

[6] M. Choi, J. J. Oh, and S. B. Choi, "Linearized recursive least squares methods for real-time identification of tire–road friction coefficient," *IEEE Trans. Veh. Technol.*, vol. 62, no. 7, pp. 2906–2918, Sep. 2013.

[7] M. Doumiati, A. C. Victorino, A. Charara, and D. Lechner, "Onboard real-time estimation of vehicle lateral tire–road forces and sideslip angle," *IEEE/ASME Trans. Mechatronics*, vol. 16, no. 4, pp. 601–614, Aug. 2011.

[8] J.-O. Hahn, R. Rajamani, and L. Alexander, "GPS-based real-time identification of tire-road friction coefficient," *IEEE Trans. Control Syst. Technol.*, vol. 10, no. 3, pp. 331–343, May 2002.

[9] L. Li, K. Yang, G. Jia, X. Ran, J. Song, and Z.-Q. Han, "Comprehensive tire–road friction coefficient estimation based on signal fusion method under complex maneuvering operations," *Mech. Syst. Signal Process.*, vol. 56, pp. 259–276, 2015.

[10] G. Park, Y. Hwang, and S. B. Choi, "Vehicle positioning based on velocity and heading angle observer using low-cost sensor fusion," *J. Dyn. Syst., Meas., Control*, vol. 139, 2017, Art. no. 121008.

[11] J. J. Oh and S. B. Choi, "Vehicle velocity observer design using 6-d imu and multiple-observer approach," *IEEE Trans. Intell. Transp. Syst.*, vol. 13, no. 4, pp. 1865–1879, Dec. 2012.

[12] S. Han and K. Huh, "Monitoring system design for lateral vehicle motion," *IEEE Trans. Veh. Technol.*, vol. 60, no. 4, pp. 1394–1403, May 2011.

[13] Y. Lian, Y. Zhao, L. Hu, and Y. Tian, "Cornering stiffness and sideslip angle estimation based on simplified lateral dynamic models for four-in-wheel-motor-driven electric vehicles with lateral tire force information," *Int. J. Automotive Technol.*, vol. 16, pp. 669–683, 2015.

[14] Y.-H. J. Hsu, S. M. Laws, and J. C. Gerdes, "Estimation of tire slip angle and friction limits using steering torque," *IEEE Trans. Control Syst. Technol.*, vol. 18, no. 4, pp. 896–907, Jul. 2010.

[15] K. Han, E. Lee, and S. Choi, "Early detection of tire-road friction coefficient based on pneumatic trail stiffness," in *Proc. Amer. Control Conf.*, 2016, pp. 6326–6331.

[16] P. A. Ioannou and J. Sun, *Robust Adaptive Control*. North Chelmsford, MA, USA: Courier Corp., 2012.

[17] K. Han, Y. Hwang, E. Lee, and S. Choi, "Robust estimation of maximum tire-road friction coefficient considering road surface irregularity," *Int. J. Automotive Technol.*, vol. 17, pp. 415–425, 2016.

[18] R. Rajamani, G. Phanomchoeng, D. Piyabongkarn, and J. Y. Lew, "Algorithms for real-time estimation of individual wheel tire-road friction coefficients," *IEEE/ASME Trans. Mechatronics*, vol. 17, no. 6, pp. 1183–1195, Dec. 2012.

[19] J. Wang, L. Alexander, and R. Rajamani, "Friction estimation on highway vehicles using longitudinal measurements," *J. Dyn. Syst., Meas. Control*, vol. 126, pp. 265–275, 2004.

[20] K. S. Han, E. Lee, M. Choi, and S. B. Choi, "Adaptive scheme for the real-time estimation of tire-road friction coefficient and vehicle velocity," *IEEE/ASME Trans. Mechatronics*, vol. 22, no. 4, pp. 1508–1518, Aug. 2017.

[21] S. Lee, K. Nakano, and M. Ohori, "On-board identification of tyre cornering stiffness using dual Kalman filter and GPS," *Veh. Syst. Dyn.*, vol. 53, pp. 437–448, 2015.

[22] C. Lundquist and T. B. Schön, "Recursive identification of cornering stiffness parameters for an enhanced single track model," *IFAC Proc. Vol.*, vol. 42, pp. 1726–1731, 2009.

[23] K. Berntorp and S. Di Cairano, "Tire-stiffness estimation by marginalized adaptive particle filter," in *Proc. IEEE 55th Conf. Decision Control* , 2016, pp. 2443–2448.

[24] G. Baffet, A. Charara, and D. Lechner, "Estimation of vehicle sideslip, tire force and wheel cornering stiffness," *Control Eng. Practice*, vol. 17, pp. 1255–1264, 2009.

[25] R. Rajamani, *Vehicle Dynamics and Control*. New York, NY, USA: Springer, 2011.

[26] H. Pacejka, *Tire and Vehicle Dynamics*. New York, NY, USA: Elsevier, 2005.

[27] C.-S. Kim, J.-O. Hahn, K.-S. Hong, and W.-S. Yoo, "Estimation of tire–road friction based on onboard 6-DoF acceleration measurement," *IEEE Trans. Veh. Technol.*, vol. 64, no. 8, pp. 3368–3377, Aug. 2015.

[28] K. Nam, H. Fujimoto, and Y. Hori, "Advanced motion control of electric vehicles based on robust lateral tire force control via active front steering," *IEEE/ASME Trans. Mechatronics*, vol. 19, no. 1, pp. 289–299, Feb. 2014.

[29] D. Simon, *Optimal State Estimation: Kalman, H Infinity, and Nonlinear Approaches*. New York, NY, USA: Wiley, 2006.

Kyoungseok Han received the B.S. degree in civil engineering (minor in mechanical engineering) from Hanyang University, Seoul, South Korea, in 2013, and the M.S. degree in mechanical engineering from the Korea Advanced Institute of Science and Technology, Daejeon, South Korea, in 2015, where he is currently working toward the Ph.D. degree in mechanical engineering. His current research interests include vehicle dynamics and control, optimization problems, and control theories.

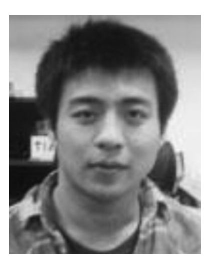

Mooryong Choi received the B.S. degree in mechanical engineering from Yonsei University, Seoul, South Korea, in 2008, the M.S. degree in mechanical engineering from the University of California, Los Angeles, CA, USA, in 2010, and the Ph.D. degree in mechanical engineering from the Korea Advanced Institute of Science and Technology, Daejeon, South Korea, in 2014. He is currently at the Korea Railroad Research Institute, Uiwang, South Korea. His research interests include vehicle dynamics, control, and computer vision.

Seibum B. Choi (M'09) received the B.S. degree in mechanical engineering from Seoul National University, Seoul, South Korea, in 1985, the M.S. degree in mechanical engineering from the Korea Advanced Institute of Science and Technology (KAIST), Daejeon, South Korea, in 1987, and the Ph.D. degree in control from the University of California, Berkeley, CA, USA, in 1993. From 1993 to 1997, he was involved in the development of automated vehicle control systems at the Institute of Transportation Studies, University of California. In 2006, he was with TRW, Warren, MI, USA, where he was involved in the development of advanced vehicle control systems. Since 2006, he has been with the faculty of the Department of Mechanical Engineering, KAIST. His current research interests include fuel-saving technologies, vehicle dynamics and control, and active safety systems.

Authorized licensed use limited to: Korea Advanced Inst of Science & Tech - KAIST. Downloaded on March 06,2020 at 10:35:29 UTC from IEEE Xplore. Restrictions apply.